Trends in Neuroscience and Education 15 (2019) 48–61

Contents lists available at ScienceDirect

Trends in Neuroscience and Education

journal homepage: www.elsevier.com/locate/tine

Research paper

Distributed neural efficiency: Intelligence and age modulate adaptive allocation of resources in the brain

Kanchna Ramchandran, Eugene Zeien, Nancy C. Andreasen

University of Iowa, Department of Psychiatry, Carver College of Medicine, 200 Hawkins Drive, Iowa City, IA 52242, United States

ARTICLE INFO

Keywords:
Neural efficiency
Task-related dynamic functional connectivity
Fmri
Fluid intelligence

ABSTRACT

Whether superior intelligence is associated with global lower resource consumption in the brain remains unresolved. In order to tap fluid intelligence "Gf" cortical networks, 50 neurologically healthy adults were functionally neuro-imaged while solving a modified version of the Raven Advanced Progressive Matrices. "Gf" predicted increased activation of key components of the dorsal attention network (DAN); and age predicted extent of simultaneous deactivation in key components of the default mode network (DMN) during problem-solving. However, there was no significant difference in mean levels of whole brain activation even when cognitively taxed. This suggests that the brain may dynamically switch resource consumption between these anti-correlated DAN and DMN networks, concentrating processing power in regions critical to enhanced cognitive performance. We term this mechanism of activation increase and decrease of these anti-correlated DAN/DMN systems, modulated by "Gf" and age, as "distributed neural efficiency". This may achieve local cost-efficiency trade-offs, while maintaining global energy homeostasis.

1. Introduction

A neural efficiency hypothesis (NEH) proposes that better cognitive performance is associated with lower global cortical energy consumption [1,2]. While early studies supported the NEH, later ones have suggested moderating variables such as age, gender [3,4], task type, task demands [5], training, task familiarity and brain area [6]. An alternate view has emerged, suggesting that the NEH is valid when task difficulty is moderate to low, but that when highly challenging cognitive tasks are performed, task-specific brain regions rise to the challenge and consume more energy [5,6].

It is suggested that neural efficiency declines in older adults, where there may be compensation-related utilization of neural circuits (CRUNC−Hypothesis) resulting in either over or under-activation of neural circuits involved in cognitive processing [7]. Fluid intelligence or "Gf" [8], known to decline with age [9,10], is vital for adaptive response to novelty and is relatively independent of learning and prior knowledge. The aging process may be linked to the gradual reduction of energy sources such as ATP (adenosine triphosphate) which creates cascading events of metabolic slowdown and dysfunctions that result in structural degeneration [11]. Thus aging individuals who may be experiencing metabolic slowdown, may be additionally challenged in brain function when attempting to acquire new skills or learn new information, a topic of relevance to gerontological education [12].

Hence, we focus our attention in this study on how neural efficiency may be modulated by age and fluid intelligence as task challenge increases in a functional imaging resonance (fMR) study assessing "Gf". In this fMR task, we examined levels of brain activity by measuring the BOLD (blood oxygenation level dependent) response when people perform an increasingly challenging test of mental agility that tests "Gf". There is emerging evidence that the BOLD signal is strongly coupled with the metabolic demands of adjacent neural activity in both experimental conditions and when computationally modeled [13–15]. Hence the extent of signal change of the BOLD response in this task, may putatively and indirectly assay extent of brain resource consumption and energy expenditure.

The largest metabolic energy cost in the human cortex is expended towards synaptic transmission [16] in information processing during both during baseline resting states and in external task processing. While there are significant regional changes in oxidative metabolism, the brain barely consumes any extra energy [17–20] during external task processing, than at baseline. This may be facilitated by the presence of energy-efficient neural information processing systems range across multiple levels of organization ranging from action potentials and axonal conduction at the neuronal level, to energy –efficient dynamics at the circuit level, and efficient functional connectivity dynamics across/within neuronal circuits and networks [21].

Approximately 20% of the brain's oxygen intake and 25% of its

E-mail address: kanchna-ramchandran@uiowa.edu (K. Ramchandran).

https://doi.org/10.1016/j.tine.2019.02.006
Received 13 July 2018; Received in revised form 18 January 2019; Accepted 27 February 2019
Available online 19 March 2019

glucose consumption is utilized towards complex cognitive task processing, and almost all the brain's oxygen consumption is driven towards oxidative glycolysis, the major substrate of the brain's energy metabolism [22–24]. Oxidative metabolism, the focus of the studies above, is almost exclusively funneled into oxidative glycolysis, largely for maintaining excitatory/inhibitory (E/I) balance of glutamate and gamma-aminobutyric acid (GABA) signaling [21,22].

Eighty percent of the brain's energy maintains the (E/I) balance of glutamate/GABA signaling [25] and is consumed at baseline resting state when the brain is engaged in internally focused information processing, at a network of brain regions that are intrinsically active [26–28]. This is a condition first referred to as “REST” or “random episodic silent thought” [29] which activates regions known as the default mode network (DMN) (Fig. 1). The brain's energy consumption during “REST” also supports glial functions and various processes such as biosynthesis and redox regulation [30], all of the above being very metabolically expensive. These may be some of the reasons why there is only a marginal increase in global energy consumption during externally focused cognitive processing [22,25]. When the human brain is focused on external task processing, it activates a network of regions called the dorsal attentional network (DAN) [31].

Several brain regions are implicated in cognitive intelligence [32–34] according to an overarching theory of intelligence, the Parieto-frontal integration theory (P-FIT) [35]. They include key nodes of the DAN namely, Brodmann’ s Area (BA)7/precuneus/superior parietal lobule (SPL) and the dorsolateral prefrontal cortex (DLPFC), which together form a fronto-parietal attentional control system [31] and oversees external task processing. The P-FIT theory, also includes key nodes of the DMN, namely BA10/medial prefrontal cortex (MPFC) and the posterior cingulate (PC) [36] that have high metabolic activity during internally focused processing when the brain is at rest. These 4 brain nodes (Fig. 1) have some of the highest glycolytic indices in the brain [30] and are part of an updated P-FIT system of intelligence [36] that is facilitated by high, structural, white matter interconnectivity between themselves and the rest of the brain (high centrality) [37]. We focus our attention on these four hubs in this exploratory study for the reasons mentioned above and because they represent the peak co-ordinates of BOLD activation in our fMR task.

These above mentioned nodes form important hubs [38] in a densely connected neural grid called the rich club network [39] that allows fast and efficient communication between disparate parts of the brain [40]. There is emerging evidence indicating that these P-FIT nodes also represent flexible hubs [41] that can modulate their functional connectivity rapidly to accommodate a wide variety of cognitive demands. It appears that these hubs have the highest global functional connectivity across the brain, placing them in a unique relationship vis-a-vis themselves as well as relative to other networks, in facilitating adaptive task control [42]. Amongst these P-FIT hubs, individual differences in the global, functional connectivity of the DLPFC is linked to fluid intelligence and cognitive control [43]. While the DMN nodes are characterized by spontaneous quietening (task negative) when the brain is engaged in externally focused processing, there is also emerging evidence that the both DMN and DAN nodes display some of the highest flexibility (amongst large-scale brain networks) in reconfiguring their functional connectivity. Thus, they can also co-activate in unison when solving tasks with high levels of cognitive demand [42]. While global efficiency of the overall functional brain network is not associated with intelligence, nodal efficiency of some of the P-FIT hubs are either positively or negatively correlated with IQ [44].

Cost-efficiency analyses of the two networks of DMN and DAN reveal that they maintain the highest costs of remaining hyper-connected at rich club nodes and that these wiring costs and resulting high metabolic demand directly predict cognitive performance [45]. However, it appears that individuals with higher intelligence tend to have lower dendritic intensity and arborization in gray matter, perhaps fostering neural efficiency through more directed processing through the P-FIT regions and not through overall cortical activity [46].

Healthy aging is known to result in reconfiguration of connectivity between and within large-scale networks. Keeping with age-related functional dedifferentiation, older adults show lower modularity, lower local efficiency and lower intra-network functional connectivity of the DMN [47]. Additionally, in a study of short-term dynamic functional connectivity and cognitive performance in older adults, those older adults who could maintain a longer time-span of a dynamic connectivity pattern with high DMN connectivity, also performed better on tests of executive function [48].

An important aspect of “Gf” is working memory, whose performance is shown to be directly associated with the E/I balance in the brain [49], which is metabolically expensive. Thus higher working memory performance is directly correlated to a lower GABA to glutamate ratio in the frontal cortex and lower glutamate levels in the occipital cortex, putatively indicating that the brain may be distributing energy cost/benefit ratio across brain regions [50]. Since keeping working memory online in the frontal cortex may incur higher energy costs, perhaps a tradeoff is effected by simultaneously lowering glutamate levels elsewhere in the brain (occipital cortex).

Hence, we explore the possibility that mechanisms of neural efficiency at the circuit/network level in the brain [21], may involve reorganization of metabolic resources to accommodate the decline of fluid intelligence with age. This may be related to a distributed system of E/I and cost/benefit energy ratios in relation to “Gf” across brain regions, since “Gf” is compromised with age related metabolic

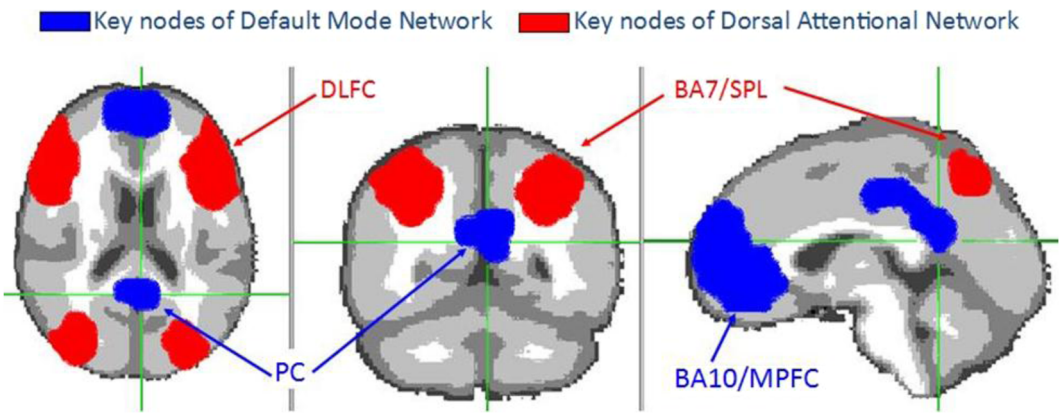

Fig. 1. Key nodes of default and dorsal attentional networks: Illustration of key nodes of the default mode network namely, Brodmann Area (BA) 10 extending into the medial prefrontal cortex (MPFC) and the posterior cingulate (PC); Also, key nodes of the dorsal attentional network, namely Brodmann’s Area (BA) 7 or the precuneus extending into the superior parietal lobule (SPL). The green cross hairs locate the regions across the three sections of the brain.

slowdown. Additionally, age-related reconfiguration of network connectivity at baseline as well as during complex cognition involving external tasks, may be taking place.

Thus, we hypothesize and explore the possibility that when the brain is cognitively loaded, it may be able to (1) toggle resources from the DMN nodes to key nodes of the DAN network such as the SPL and DLPFC, which are charged with task performance; and (2) draw upon additional activation from normally quietened DMN nodes (during external task performance), especially in the PFC, if needed. Thus, the brain may be able to maintain overall homeostatic balance and neural efficiency by a system of distributing resources just in time, to those hubs that are involved in task processing while simultaneously quietening redundant nodes. Hence, this study directs its attention at exploring a potential distributed mechanism of neural efficiency between key nodes of these two major neuronal networks, the DMN [28] and the DAN [31]. We further explore how fluid intelligence or "Gf" [8], age, and task difficulty may modulate this distributed mechanism of neural efficiency.

Sex has also been proposed as a moderator of neural efficiency [6] in the literature. Structural imaging has indicated sex differences in (a) gray matter regions and (b)white versus gray matter associated with IQ [51] indicating that intelligence may be achieved by different sex-related structural brain designs. Sex differences have also been associated with regional differences in activation patterns in cognitive reasoning [52], but these studies do not directly examine sex differences in the context of neural efficiency. Thus, as a corollary to our main focus, we additionally explore if sex is significantly correlated with the BOLD response and behavioral variables in our data, along with the extant moderators of age, "Gf" and task difficulty.

2. Materials and methods

Participants: We studied 50, cognitively average to high functioning individuals (Mean Full scale Intelligence quotient = 122.4, SD = 16.47, minimum = 88, maximum = 155), measured with the Wechsler Adult Intelligence Scale-WAIS –III [53]. These participants ranged in education from 12 to 20 years (Mean = 17.08 years of education, SD = 2.5). There were 32 males and 18 females with average age of 47.6years (SD = 15.55, minimum = 18 years, maximum = 73 years). Forty-nine participants were of Caucasian ethnicity, with one Asian Indian. fMR scan parameters: Functional imaging was performed with a Siemens 3T TIM Trio scanner using a 12-channel head coil. T1-weighted images were acquired using a spoiled grass sequence obtained with the following parameters: 1.0-mm coronal slices, 10° flip angle, TR 25 milliseconds (ms), TE 40 ms, NEX 1, FOV 26 cm, and 256 × 256 matrix. The blood oxygenation level dependent (BOLD) technique [54] with an EPI paradigm was utilized with the following T2* parameters: TR 2 s; TE 30 ms; matrix size 64 × 64; FOV 24 × 24 cm. Twenty-seven 5-mm slices were acquired, covering the entire cerebrum.

Task scanning parameters: The fMR paradigm task consisted of 21 visuo-spatial matrix problems drawn from the Raven's advanced progressive matrices (RAPM) [55] programmed on E-prime software [56]. The RAPM is a culture-free, non-verbal measure that is a prototypical measure of "Gf." Prior to scanning, participants were pre-exposed to the task on a computer screen, using RAPM Set 1 and the control task, to familiarize them with testing procedures. Each RAPM was a 3 × 3 matrix where the lower right element was missing. The cells could vary left right, up down, diagonally, or a combination there of. Some patterns were subtractive, additive, and/or rotational. Solutions were presented as two rows of four unique cells for eight options. In the control task, which began and ended each RUN, six simple 3 × 3 matrices were presented consecutively for 4 s each. All the elements in the simple matrix were identical except the empty lower right cell. Participants were given two options wherein either the top or the lower row was entirely correct. Eight 24-second control tasks alternating with seven RAPM tasks completed a RUN.

During scanning, subjects were shown matrices 1–21 from Set 2 of the RAPM, with seven matrices per RUN, each progressively more difficult. The RAPM Set 2 is constructed in such a way that each matrix from 1–21, gets progressively more complex in their underlying rules, and hence RUNS 1, 2 and 3 are progressively more difficult to solve. Task difficulty increased with matrix complexity, and limiting the time allowed to solve each RAVEN matrix to 40 s escalated the challenge. Participants were instructed to continue pondering the RAPM matrix for the full 40-second duration and change their answers as needed. The average correct responses for the RAPM puzzles in RUNS 1, 2 and 3 were 4.66, 3.24, and 2.66 respectively, with the number of correct responses dropping off as each RUN became progressively more difficult. We also calculated the total number of correct responses from the 21 RAPMs (across three RUNS), as reflective of the participant's fluid intelligence (Gf) score known as RAVENIQ henceforth.

Thus, three RUNS of fMR scans were completed consecutively in the scanner with each RUN being 7 min, 54 s in duration, with a total of 237TRs of fMRI data collected per RUN. The upper row of available responses in each matrix was linked to the right-hand manipulandum (response recording device that the palm/fingers rest on), the lower row to the left, and participants responded through task buttons for each finger. When the participants were satisfied that they had discerned the pattern, they pressed the button corresponding to one of the eight options.

Data pre-processing and Image analysis: This was conducted using Analysis of Functional Neuroimages (AFNI) [57]. Individuals' data were slice-time corrected via *to3d's alt+z option*. *3dDespike* was used to remove random noise artifacts of obnoxious amplitude. The "best" volume of the 4D series was identified by *3dTqual* and used as the base for *3dvolreg* intra-series motion correction. Each series was spatially smoothed via *3dmerge* with a 10.5 mm FWHM Gaussian filter. Our voxel size was 3.5 mm. Thus our filter size was adjusted to be approximately 3 times the voxel size in order to simultaneously cluster homologous anatomic regions and yet separate functionally distinct regions [58]. This had additional advantages. It (1) reduced the number of independent regions or number of tests and hence decreased noise, (2) increased overlap for group results between participants, and (3) provided a strong visual aid in Fig. 3, in presenting the spatial expanse of de-activation between RUNS1, 2 and 3.

Normalization was then simply performed by dividing by the series mean, and then multiplying by 100. Since this was a block design rather than event-related, the next step was to apply a low-pass filter (*3dFourier* -low pass 0.08333 *-retrend*) to remove high frequencies. As the last step, the three RUNS were concatenated within *3dDeconvolve*. In doing so, *3dDeconvolve* modeled the three RUNS as separate instances for noise & trends.

This experiment was originally conceived as an A/B (RAPM/control) block design. While reviewing individuals' BOLD signal within the RAPM positive activation regions, a third component was revealed which corresponded temporally to the last response within the RAPM block. To explore this, an A/B/C block model was created wherein time from subjects' last response within an RAPM matrix block to the onset of the next control matrix was assigned to C. Please refer to Fig. 2 for a timing diagram of this quasi event-related design method. The result revealed an activation pattern during C very similar to the DMN (default mode network) found in many studies of resting subjects, and lent credence to the modified A/B/C model. The output of each participant's *3dDeconvolve* consisted of t-statistics for conditions A, B and C of the model. Average time to last response within each RAVEN block was 25.3 s (9.5 S. D) with 2.5% of no responses. "No response" RAPM trials were modeled as RAPM for the full 40 s duration. The early RAPM matrices are relatively easy, and induced quick responses. The later, more difficult RAPM matrices garnered a mix of slow and quick responses. Overall, the quick responses outnumbered the slow, which resulted in a saw-tooth waveform when modelling time spent in RAPM (Fig. 5). All participants were "in" RAPM mode for the first few of the

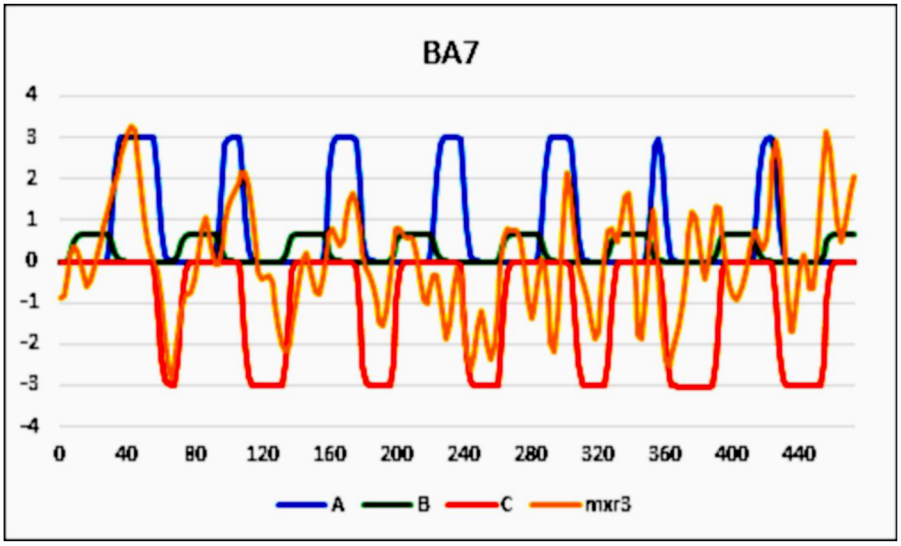

Fig. 2. Timing model of the quasi event-related design: This represents the analytic design and timing model from a random participant's activation pattern during RUN 3 (highest task difficulty) at Brodmann's area 7, which is the key area of activation in this task. The y-axis represents times in seconds from the start of RUN 3 and presents seven RAPM matrices. The X-axis represents the signal change. The RAPM task (A) ends with the participant's last response, though each matrix is presented for 40 s. Each control task (B) consists of six consecutive simple matrices with eight sets of (B). C represents time from the participant's last response in A to the onset of B. "mxr3" is the participant's BOLD signal in BA7 during RUN3.

40 s, but the tally of those still "in" dropped over its duration. The rarity of "no response" trials permitted differentiating between the end of RAPM and initiation of the control task, since the transitions were desynchronous. Thus the effects of timing were controlled in the calculation of percent signal change in order to arrive at a fairly robust measure of individual differences in activation intensity [59].

Group statistical analyses: The group's whole-brain, mean t-statistics was computed from each participant's *3dDeconvolve* output, to determine whether it varied significantly during the RAPM and control task performance. Fig. 3 visualizes this output in each of the three RUNS, while Fig. 4 displays this in RUN 3 and splits activation of the DLPFC into two separate bilateral nodes at a higher threshold. As part of the statistical analysis, we also generated the peak co-ordinates using *3dANOVA* (in AFNI), the results being listed in the results section in Table 1. The 4 areas of bilateral activations of BA7/SPL, BA10/MPFC, DLPFC and PC were selected for further analysis since they represented the regions of peak activations. We did not include the occipital lobe activity (Table 1) in any of the analyses since it was not central to our hypotheses and since activity in this cortex may be expected due to the fact that RAPM task involves visual pattern recognition. We also calculated the percent signal change from beta-coefficients, for each of the 4 regions of interest (ROI), based on peak voxel activation, selected by AFNI [57] recorded in Table 2. This was subsequently used for further statistical analyses. The actual and idealized hemodynamic responses of the participants during the control and RAPM tasks at each of the four nodes of interest are displayed as wave-forms in Figs. 5 and 7. They serve as a simplified indicator of time-stamped activity in each of these nodes (Fig. 5) and split by top and bottom 1/3rds of the group's "Gf" and "age" in Fig. 7.

In order to test both the main effects as well as the interactions between "Gf" (RAVENIQ) and age in the context of task difficulty (RUN1 and RUN 3) on extent of activation (percent signal change) we performed multiple, multivariate analyses of variance (MANOVA), one for each region of interest (ROI). The Pillai-Bartlett statistic was reported for those tests that attained statistical significance on the MANOVAs. Secondary univariate ANOVAs were generated to examine main and interaction effects of RAVENIQ and age for RUN1 and RUN3 separately since they represented the easiest and most difficult of task conditions respectively. Post –hoc Wilcoxon tests were performed as well, to examine if the percent signal changes between RUN1 and RUN3 repeated measures, were significantly different. Statistically significant results from the multivariate, univariate analyses, and the Wilcoxon tests are presented in Table 4. To complement these results, we additionally conducted a task-based functional connectivity analysis to examine interaction effects of the above mentioned co-variates.

Task-related functional connectivity analysis: A *3dDeconvolve* was RUN for each participant for RUNS 1 and 3 separately, seeded at BA10 and BA7 peak voxels during the RAVEN task. The associated beta coefficients for these RUNS were then fed into a multi-level model analysis using the AFNI function *3DMVM*. This model generated a group level (between subjects) ANOVA of age, RAVENIQ and RUN with an output of the interaction effects of these co-variates as well as their main effects. The within-subjects' variables were brain nodes (BA10, BA7) and RUN (1, 3). The functional connectivity patterns of these interaction effects (Fig. 6) were restricted to a mask representing DAN, DMN regions of peak activations during the RAVEN task as reported in Table 1. Additionally, we generated a general linear t-test (without masks) that examined the functional connectivity model seeded at BA7 and BA10, as a contrast between these two ROIs (BA7vs. BA10), with the co-variates of age and RAVENIQ during RUN3. This last general linear t-test was meant to starkly display the functional anti-correlations between these two ROIs when the RAPM task was at its most challenging. Fig. 6 contains the results of the task-related functional connectivity analysis.

As a secondary analysis, we were interested in examining whether there was a significant percent signal change between RAPM and control task in the whole brain, which would serve as an indicator of whether the brain maintained similar levels of whole-brain activation irrespective of cognitive load. Towards this end, we first calculated the non-normalized, whole brain activation/de-activation peak coordinates in individuals' processed 4D images, and then performed a group level analysis of variance (ANOVA) of these extracted whole brain percent signal changes between the control task (very easy) and the RAPM (very difficult). Since spatial normalization tends to compress/limit whole brain activation/de-activation peak co-ordinates, we used non-normalized brain data in order to perform this additional/secondary analysis.

We also generated two Pearson's correlation coefficient [60] matrices, the first of whose purpose was to examine the relationships between demographic variables of interest in this study such as age, gender, sex and education, all of which have been known to impact neural efficiency [6], with measures of intelligence such as "Gf-RAVENIQ" and WAIS IQ. This was also correlated with response times in RUNS1 through 3. The results are presented in Table 3. The second correlation coefficient table examined the relationships between percent signal change in the key brain regions of interest with RAVENIQ, sex and age, at RUN 1 and RUN 3, which represent the easiest and the most difficult of task conditions respectively. This second correlation coefficient matrix is presented in Table 2.

All group level statistical analyses were performed using R Studio software [61].

3. Results

Our first set of results dissect the activation patterns of the fMR analysis of whole brain activity (RAPM vs. control task) of all 3 RUNS. This indicates a significant ($q < 0.001$, 2-tailed) increase in BOLD response at the SPL/BA 7 and DLPFC (Fig. 3), the core processing areas for visuo-spatial problem-solving in the RAPM, as observed in previous studies [2,62,63]. The DLPFC is also activated in this task (Fig. 3), which together with BA7 form critical sections of the DAN [64] as seen in Fig. 1.

Panel A in Fig. 3 suggests that the RAVEN task is processed primarily in the DLPFC, superior parietal cortex, primary and extra-striate visual cortices in RUN1, when the puzzles are the easiest to solve. As they get harder to solve in RUNS 2 and 3 respectively, the BA7/precuneus appears to be recruited as well in problem solving. The peak activation co-ordinates across all three RUNS are available in Table 1. Of greater interest though is the increasing spatial expansion of the de-activation or suggested suppression of two key nodes of the DMN network, the BA10/MPFC and the posterior cingulate, as the task progresses in increasing difficulty from RUN 1 to RUN 3 (Fig. 3, Panel A-C).

We calculated the percentage of signal change (Table 2) during the RAPM blocks from peak voxels in each of these regions (BA 7, 10, DLPFC and PC) as reflective of the metabolic activity in these areas for RUN 1 and RUN3 (representative of the simplest and most difficult respectively).

The difference in extent of de-activation (difference in percent signal change) between RUN 1 and RUN3 at the two DMN nodes reaches statistical significance both at the BA10/MPFC ($r = 0.54$, $p < 0.01$) and at the PC with $r = 0.93$, $p < 0.0.001$ (see Table 2). For the key DAN ROIs, there is a significant increase in percent signal change between RUNS 1 and 3, as reported in Table 2, at both the BA7/SPL/precuneus ($r = 0.66$, $p < 0.001$) and DLPFC ($r = 0.71$, $p < 0.001$).

Fig. 4, generated at a significantly higher threshold (q161-169 < 0.0001) than Fig. 3 ($q < 0.001$), shows indicates that DLPFC activations in Fig. 3, consist of two, separate nodes (Fig. 4), the anterior middle frontal gyrus (aMFG) and posterior (pMFG) while solving the RAPM matrix puzzles. Prior research [66], has indicated that activation of the pMFG node serves as a central executive that regulates and spurs negative functional connectivity between the DMN nodes of MPFC/PC and specific DAN nodes (superior parietal lobule/precuneus, DLPFC.) We simultaneously see activity in the aMFG as well (Fig. 4), which along with the pMFG is known to strengthen connectivity [66] between the DLPFC and superior parietal lobule/precuneus (DAN nodes). Hence, we may putatively infer that during the RAPM task, activation of pMFG may trigger the anti-correlation between the DAN and DMN nodes while strengthening the connectivity between the DAN nodes especially during RUN3 when the puzzles are hardest to solve.

These DMN and DAN nodes targeted in this study appear to be anti-correlated during task performance as visualized in Fig. 5. As evident in Table 2 and visually apparent in Fig. 3, BOLD response decreases (as does percent signal change) at BA 10/MPFC and PC, and spatially expands from RUN1 to RUN3, as task difficulty escalates. RUN3 sees a parametric increase in percent signal change (Table 2) and increased area under the curve in Fig. 5 in BA7 and DLPFC (comprising the DAN) compared to RUN1, when the matrices are being solved. We also see a parametric decrease in percent signal change in MPFC and PC in Table 2, between RUNS1 and 3. This decrease in percent signal change is visually apparent as increasing/spatially expanding de-activations/suppression at BA10 and PC in Fig. 3 between RUNS 1 and 3. These are also visualized as deepening troughs at BA10 and PC between RUNS 1 and 3 (Fig. 5) during the RAPM task. In addition, when the brain is minimally processing the control task (which is very easy), we see in

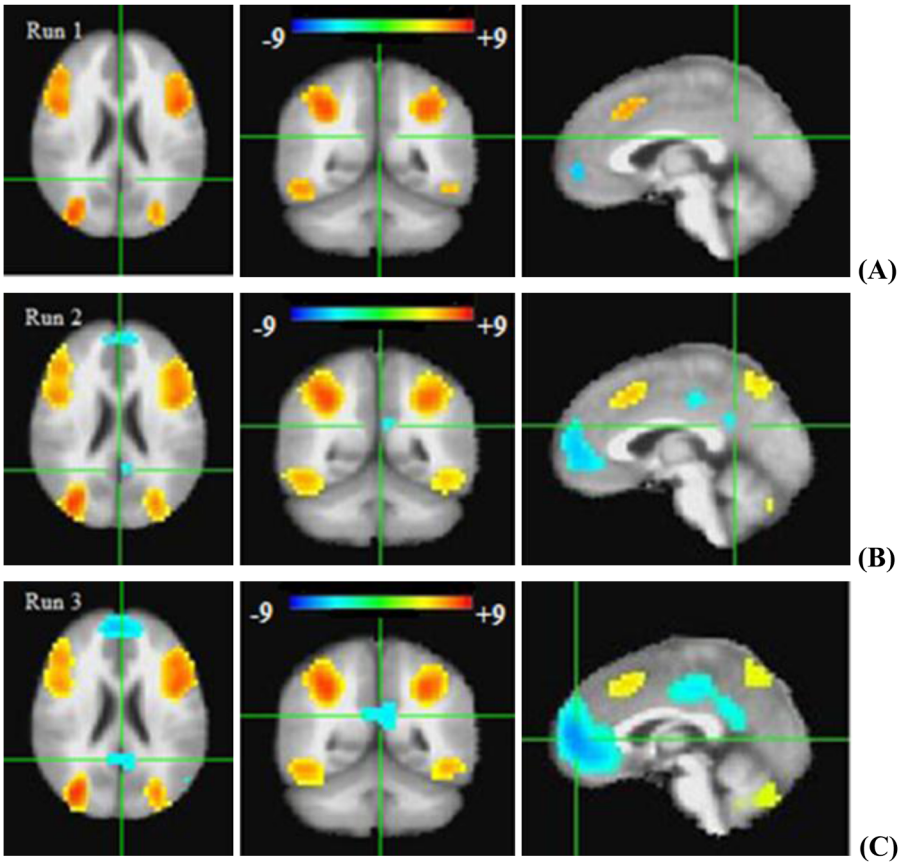

Fig. 3. Activation pattern on RAPM task across 3 RUNS. t-statistic ($q < 0.001$, OLSQ-ordinary least square) of activation pattern of the RAPM task progressing from RUN1(panel A), RUN 2 (panel B) RUN 3(panel C), with decreasing BOLD activity from RUN 1(easier tasks) to RUN 3 (most difficult tasks) at Brodmann area (BA) 10/medial prefrontal cortex (MPFC) and posterior cingulate; and positive, increased activation at superior parietal lobule, Brodmann' s Area (BA) 7/precuneus, extra striate cortex, visual cortex and dorsolateral pre-frontal cortex (DLPFC). These are all core regions of the P-FIT [65]. This figure displays the progression in de-activation in the key DMN nodes and increased activation of the DAN nodes, as the RAPM task ramps up difficulty from RUN1 to RUN3.

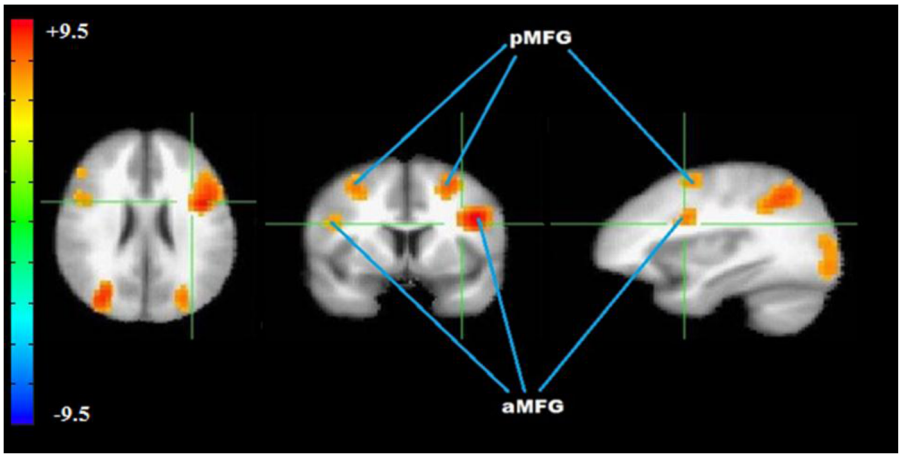

Fig. 4. Dual nodes of the middle frontal gyrus. Left to right are the axial, coronal and sagittal views of the T-statistic ($q < 0.0001$), in RUN3, averaged across all participants while solving the matrices. Highlighted in the frames are the anterior and posterior middle frontal gyri respectively titled as aMFG and pMFG.

Table 1
Peak co-ordinates of activation patterns in the RAPM task. *Talairach co-ordinates with center of mass (CM) and peak voxels for sagittal (x), coronal (y), and axial (z) planes are provided.*

Brain region	Voxels	Volume (cc)	CM x	CM y	CM z	Peak x	Peak y	Peak z
Bilateral Superior Parietal Lobe	3194	135.77	−4.1	65.1	15.8	−26.2	65.2	44.2
(Left Dorsolateral Prefrontal Cortex)	1083	46.04	32.8	−14.5	29.9	43.8	−4.8	26.8
Left Inferior Frontal Gyri								
Left Middle Frontal Gyri								
(Bilateral Medial Prefrontal Cortex)	983	41.79	−0.2	−47.7	8	−1.8	−53.8	2.2
Bilateral Medial Frontal Gyri								
(Right Dorsolateral Prefrontal Cortex)	540	22.95	−42.2	−12.1	29.4	−47.2	−4.8	23.2
Right Inferior Frontal Gyri								
Right Middle Frontal Gyri								
Bilateral Cingulate & Posterior Cingulate Gyri	380	16.15	0.3	35.6	28.5	−1.8	26.8	37.2
Left Occipital Gyrus	69	2.93	57.1	17.6	−11.7	57.8	12.8	−15.2
Right Occipital Gyrus	23	0.98	−34.4	−22.1	−1.2	−33.2	−22.2	−1.2

Table 2
Correlation (Pearson r) matrix of "Gf" with activity in key brain nodes. *"Gf" is represented by RAVENIQ (total correct responses in the RAVEN task performed in the MRI scanner). Brain activity in the key nodes of the dorsal attention network are dorsolateral pre-frontal cortex (DLPFC), Brodmann's area (BA) 7/precuneus/superior parietal lobule, and in the default mode network are Brodmann' s area (BA)10/medial prefrontal cortex, posterior cingulate(PC). Average percent signal change in these nodes during the easy (RUN1) and most difficult (RUN3) RAVEN matrices represent brain activity and are displayed in the first column on the left.*

Average% age Signal Change	Sex	Age	RAVEN IQ	BA10 RUN1	BA10 RUN3	BA7 RUN1	BA7 UN3	DLPFC RUN1	DLPFC RUN3	PC RUN1
Sex										
Age	−0.06									
RAVENIQ	−0.06	−0.4								
BA10 RUN1	−0.04	0.26	−0.19							
−0.21										
BA10 RUN3	−0.1	0.53**	−0.37	0.54**						
−0.339										
BA7 RUN1	−0.03	−0.36	0.42	−0.51**	−0.44					
0.325										
BA7 RUN3	−0.001	−0.45*	0.39	−0.44	−0.52**	0.66***				
0.421										
DLPFC RUN1	−0.08	−0.31	0.47*	−0.34	−0.33	0.70***	0.65***			
0.295										
DLPFC RUN3	0.12	−0.24	0.45*	−0.33	−0.37	0.46*	0.72***	0.71***		
0.334										
PC RUN1	−0.01	0.36	−0.03	0.13	0.15	−0.3	−0.34	−0.31	−0.19	
0.8030										
PC RUN3	0	0.37	−0.03	0.16	0.17	−0.33	−0.35	−0.27	−0.18	0.93***
0.725										

* Correlation is significant at 0.05 levels (2-tailed).
** Correlation is significant at 0.01 levels (2-tailed).
*** Correlation is significant at 0.001 levels (2-tailed). *Correlation is corrected for multiple comparisons using the Holms method.*

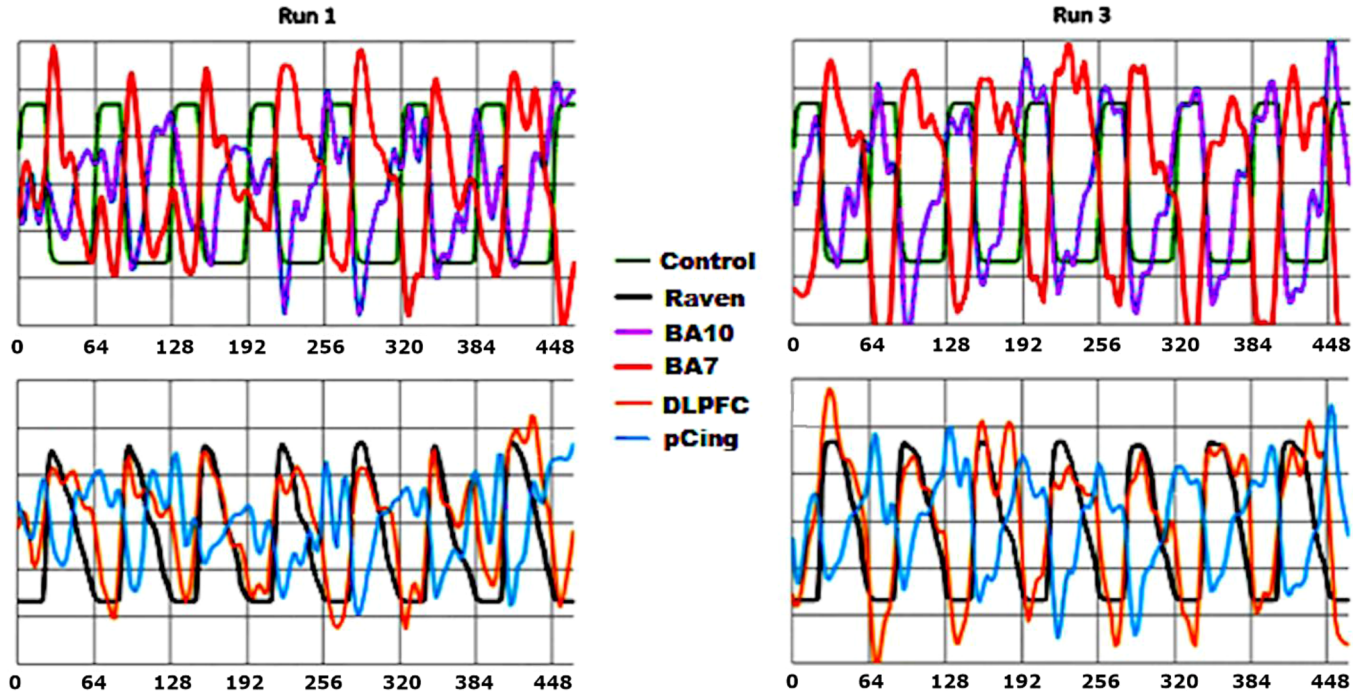

Fig. 5. Oscillatory waveforms of hemodynamic response at key nodes of Parieto-frontal intelligence theory (P-FIT) network. This figure displays the anti-correlated nature of the wave-forms of the key ROIs of the Dan. DMN networks during the RAPM. The Raven model presented is a composite of all participants in RUN1 and RUN3. All signals are arbitrarily scaled for easy visual comparison around zero (Y-axis). The X-axis represents time from start of functional scan to completion of a RUN. The X-axis is calibrated in intervals of 64 s: each control task blocks (green-24 s) + RAVEN experimental task block (black-40secs). Each RUN commences with the control task and alternates with seven RAVEN matrices. None solved each matrix in less than 2 s, and 2.5% of participants consumed the full 40 s allowed. The idealized hemodynamic response function (HRF) of the control task and the RAPM are represented as a backdrop for the actual hemodynamic responses (wave-form) at the specific regions of interest: Brodmann's area (BA) 7 (superior parietal lobule/precuneus), DLPFC (dorsolateral prefrontal cortex), (BA) 10 (fronto-polar cortex/ medial prefrontal cortex) and posterior cingulate (PC).

Fig. 5 that the MPFC and PC (comprising the DMN) rise to normal levels instantaneously, indicating that activity in these regions may have been temporarily shut off while solving the matrices, and they instantaneously recover when the RAPM task is disengaged.

If the BA7, the key node of activation for the RAPM, was borrowing resources from its neighboring regions during the RAPM, then we might expect to see a significant negative correlation of its percent signal change with PC (Table 2). Instead, the activation increase in BA7/ precuneus/SPL significantly correlates with a concurrent decrease of BOLD response in the bilateral fronto-polar regions (BA 10)/MPFC (see Table 2) in both RUN1 and RUN3. This putatively suggests that BA7 is perhaps borrowing metabolic resources from BA10, a distant region of the default mode network, during the RAPM task.

The activation increase in DLPFC significantly correlates positively with BA7 in both RUNS1 and 3 (Table 2) suggesting that both regions are simultaneously on task while solving the matrices. Thus, we see parametric changes in signal (area under the curve) between RUNS 1 and 3 in all 4 brain regions of interest (Fig. 5 and Table 2). The waveforms (from Fig. 5) demonstrate time-synchronized peaks and troughs between disparate brain systems (DAN and DMN nodes), suggesting a pattern of simultaneous activation and de-activation of DAN and DMN nodes respectively.

We present further results to examine the influence of the extant moderators of neural efficiency [6] such as age, fluid intelligence, sex, education and task difficulty. In the performance of the matrix puzzles, RUN3 is the hardest to solve in comparison to the previous two RUNS, as the task gets harder over time. It is of interest to note that there is no significant correlation between age and average response time (Table 3), both in RUN1 and RUN3 levels of task challenge in our dataset, thus indicating that older adults are not significantly slower in their response to increasing cognitive challenge.

We further examined the effect of age on mental resource allocation at the 4 key brain nodes of the DMN (BA10/MPFC, PC) and DAN (BA7/ superior parietal lobule/precuneus, DLFPC), which represent the areas of highest percent signal change (Table 2) and peak activation (Table 1) in this task.

In RUN1, when task challenge is lowest, there is no significant correlation between age and percent signal change in any of the four DMN/DAN nodes (see Table 2). Age is significantly negatively, correlated with the BA7/precuneus (a DAN node critical to solving the RAPM), when the puzzles are hardest to solve in RUN 3 ($r = -0.45$, $p < 0.05$) indicating that older adults are perhaps not activating the DAN nodes especially the BA7, as much as the younger subjects. They appear to engage BA10/MPFC, more than the other three P-FIT nodes of interest in this study in RUN 3, when they are challenged the most ($r = 0.53$, $p < 0.01$, Table 2). This indicates that they may instead be recruiting the DMN network, especially the BA10/MPFC to assist/ compensate in solving the matrices.

The participants' "Gf", reflected by their RAPM scores (RAVENIQ) is significantly correlated with their WAIS PIQ (Performance Intelligence Quotient) ($r = 0.55$, $p < 0.01$,) as evident in Table 3. This is not surprising given that both are measures of "Gf". RAVENIQ is significantly correlated with the DLFC, a region connected with working memory, critical to "Gf" (Table 2) in both RUNS 1 and 3.

Those with higher FSIQ (Full-scale Intelligence quotient) also tend to be more highly educated in our dataset as per Table 3 ($r = 0.54$, $p < 0.01$). Additionally, older subjects in our dataset are more highly educated (Table 3), ($r = 0.66$, $p < 0.001$), and have higher verbal intelligence as measured by their VIQ (verbal intelligence quotient), ($r = 0.44$, $p < 0.01$). Thus, in contrast to RAVENIQ, which is a measure of fluid intelligence, age is significantly positively correlated with verbal IQ, a measure of crystallized intelligence, known to be higher in older adults [9].

Sex is not significantly correlated with any of the measures in

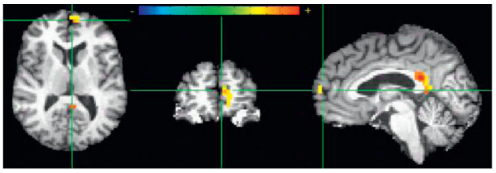

Panel A: Functional connectivity during RAPM. Interaction of age*RUN. Uncorrected $p<0.05$. Indicates functional connectivity between left posterior cingulate (F=9.82) and left BA10 (F=6.87).

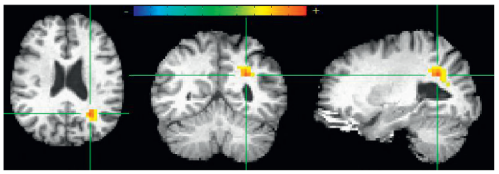

Panel B: Functional connectivity during RAPM. Interaction of RAVENIQ*RUN. Uncorrected $p<0.05$. Indicates activation at the left precuneus (F=8.89)

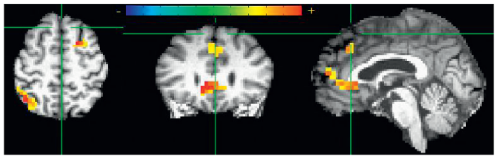

Panel C: Functional connectivity during RAPM. Interaction of age*RAVENIQ*RUN. Uncorrected $p<0.05$. Indicates activation of DAN nodes of BA7/superior parietal lobule (F=12.20) and DLPFC (F=14.83). As well as activation of DMN node of BA10/medial prefrontal cortex (F=16.23).

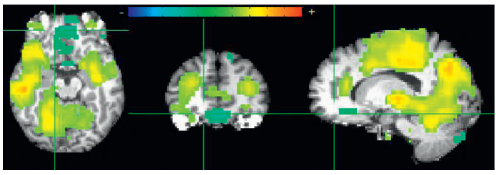

Panel D: Functional connectivity during RAPM. General Linear test of BA7 versus BA10, with the interaction of age*RAVENIQ in RUN3. T-statistic ($q< 0.05$) with deactivation of DMN node of BA10/medial prefrontal cortex with activation of extended DAN network of BA7/superior parietal lobule/precuneus and DLPFC. Displays anti-correlated functional connectivity during the hardest of task conditions.

Fig. 6. Significant results of a task-related functional connectivity analysis of a three-way interaction of age, fluid intelligence and task difficulty on activation patterns during the RAPM task. Panels A, B and C display an analysis of variance of age, fluid intelligence (RAVENIQ) and task difficulty (RUN) on functional connectivity of the DAN and DMN ROIs in this task. Results are reported at uncorrected $p < 0.05$ (given the large number of tests executed), with the corresponding F values at peak voxels of each ROI. Panel D represents the functional connectivity pattern of BA7 vs. BA10 at the hardest of all task condition (RUN3), after inputting the co-variates of age and RAVENIQ. The result reported for Panel D is that of a general linear test.

Table 3
Correlation matrix (Pearson's r) of age and fluid intelligence with psychological and other demographic variables. *Fluid intelligence is represented by RAVENIQ (total correct responses in the RAVEN task performed in the MRI scanner). The average response time while performing the Raven task across all RUNS is designated by RAVENRTav; and by RAVENRT1 and RAVENRT3 for RUNS 1 and 3 respectively. IQ measured by WAIS is provided with full scale IQ (FSIQ), performance (PIQ) and verbal IQ (VIQ).*

	Age	Sex	Education	RAVEN IQ	FSIQ	PIQ	VIQ	RAVENRT av	RAVEN RT1	RAVEN RT3
Age	1									
Sex	−0.06	1								
Education	0.66***	−0.1	1							
RAVENIQ	−0.4	−0.06	0.54**	1						
FSIQ	0.42	−0.03	−0.51	0.35	1					
PIQ	0.39	−0.1	0.15	0.55**	0.71***	1				
VIQ	0.44*	−0.05	0.58***	0.17	0.93***	0.51**	1			
RAVENRTav	−0.17	0.11	0.07	−0.03	−0.18	−0.02	−0.13	1		
RAVENRT1	−0.09	0.03	0.1	−0.13	−0.2	−0.08	−0.13	0.93***	1	
RAVENRT3	−0.16	0.11	0.09	0	−0.11	0.05	−0.08	0.91***	0.78***	1

* Correlation is significant below 0.05 levels (2-tailed).
** Correlation is significant below 0.01 levels (2-tailed).
*** Correlation is significant below 0.001 levels (2-tailed). Correlation is corrected for multiple comparisons using the Bonferroni-Holms method.

Tables 2 and 3. Since sex is not significantly correlated with percent signal change in the easy or the most difficult of task conditions (Table 2), nor any of the demographic or IQ variables (Table 3) in our data, we excluded it from further analyses, lacking statistical justification for inclusion. Since education is significantly correlated with both age and fluid intelligence (RAVENIQ), we did not include it in further analyses, to avoid multi-collinearity (Table 2).

We performed both multivariate and univariate analyses of variance (Table 4) to account for the influence of task difficulty (RUN1, RUN3) representing the easiest and most difficult of RAPM RUNS, controlling

Table 4
Analyses of variance of the effects of age, fluid intelligence and task difficulty.
Significant effects of a Multivariate Analysis of Variance (MANOVA) and univariate (ANOVA) predicting percent signal changes with increasing levels of task difficulty (RUN1, RUN3) predicted by age and fluid intelligence at relevant brain nodes of the Dorsal Attentional Network (DAN), and Default mode network (DMN).

Predictors (RAVENIQ, age) DAN - Superior parietal lobule/BA7	Pillai-Bartlett	F	df	Sum of squares	W
Multivariate					
RAVENIQ	0.22**	6.37**	2/46		
Age	0.13*	3.3*	2/46		
Wilcoxon Test (RUN1 versus RUN3)					1004.5*
Univariate RUN1					
RAVENIQ		11.12**	1	0.37	
Univariate RUN3					
RAVENIQ		9.54**	1	0.36	
Age		6.7*	1	0.26	
DAN - Dorsolateral prefrontal cortex	**Pillai-Bartlett**	**F**	**df**	**Sum Sq.**	**W**
Multivariate- RAVENIQ	0.25**	7.7**	2/46		
Univariate RUN1- RAVENIQ		13.70***	1	0.46	
Univariate RUN3- RAVENIQ		12.35***	1	0.39	
DMN - BA 10/medial prefrontal cortex	**Pillai-Bartlett**	**F**	**df**	**Sum of squares**	**W**
Multivariate					
Age	0.21**	5.942	2/46		
RAVENIQ	0.2*	4.7*	2/46		
Wilcoxon Test (RUN1 versus RUN3)					1755**
Univariate RUN 3- Age		12.12**	1	0.40	
Univariate RUN 3- RAVENIQ		9.52**	1	0.32	
DMN - posterior cingulate	**Pillai-Bartlett**	**F**	**df**	**Sum of Squares**	**W**
Multivariate- Age	0.15*	4.2*	2/46		
Univariate RUN1- Age		8.01**	1	7.7	
Univariate RUN3- Age		8.4**	1	7.07	

* significant at 0.05 levels.
** significant at 0.01 levels.
*** Correlation is significant at 0.001 levels.

for both age and RAVENIQ simultaneously in predicting percent signal change in these two RUNS. Our results (Table 4) indicate that the percent signal change of both nodes of the DMN at BA10/ MPFC and PC are significantly predicted by a main effect of age both in RUNS 1 and 3, even after controlling for fluid intelligence. In fact, there appears to be a significant difference/decrease in the percent signal change from RUN1 to RUN3 at BA10/MPFC (Table 2, Table 4-Wilcoxon Test = 1755, $p < 0.01$). Thus, our results indicate that age predicts greater deactivation in percent signal change of both key nodes (MPFC and PC) of the DMN during the RAPM task especially in RUN3.

In RUN 3, (Table 4), age as a main effect with F (1) = 6.7, $p < 0.05$, significantly predicts percent signal change in the dorsal attentional network (DAN) node of precuneus/SPL (see Table 4) when the brain is cognitively taxed the most, though to a lesser extent than RAVENIQ with F (1) = 9.54, $p < 0.01$. Age does not predict activation in the other key node of the DAN network, the DLPFC in RUN3. Although we do see a significant negative correlation between age and percent signal change at the DLPFC in RUN3 (Table 2), this drops out of significance when controlled for the influence of "Gf" (Table 4). Since the relationship between age and nodes of DLPFC and BA7/SPL are in the negative direction (Table 2) and since age predicts activity in the BA7/SPL/precuneus as a secondary effect to RAVENIQ, we may infer that older adults may not be engaging the DAN network as much as younger adults.

RAVENIQ predicts increased activation of both DAN nodes of DLPFC as well as BA7/SPL/precuneus in both RUNS 1 and 3, as a main effect (Table 4). Fluid intelligence predicts a significance increase in activation in the DAN nodes of BA7/SPL/ precuneus as the task increases in challenge between RUN1 and 3 (Table 4, Wilcoxon test = 1004.5, $p < 0.05$). RAVENIQ also predicts activity in the BA10/MPFC with F (1) = 9.51, $p < 0.01$, in the most difficult RAPM (RUN 3) as a secondary effect after age. This may imply that those with higher IQ activate the BA10/MPFC nodes less, while solving the puzzles. Thus, those with higher "Gf" may have higher metabolic activity (reflected by higher percentage signal change of BOLD response) in some of the brain's core processing areas (DLPFC and BA7/superior parietal lobule) of the dorsal attentional network, while solving RAPMs. These results suggest that participants with greater "Gf" engage the DLPFC and the BA7/SPL/precuneus while solving the matrix puzzles, irrespective of task challenge (both RUNS1 and 3).

While age has a smaller main effect in modulating percent signal change at BA7 (the key region of task processing in the RAPM) and RAVENIQ has a smaller secondary main effect in modulating percent signal change (de-activation) at BA10/MPFC, there are no significant multivariate or univariate interaction effects of RAVENIQ and age on percent signal change at any of the 4 brain nodes, examined in this analysis.

In order to directly contrast and compare the interaction effects of age, fluid intelligence and task difficulty on neural processing in the DAN and DMN during the RAPM task, a task-related functional connectivity analysis was done. In Fig. 6, Panel A indicates that the left BA10 and left PC are functionally connected during the RAPM, as an interaction effect of age and task difficulty. In Fig. 6 (Panel B), displays activation of the precuneus as an interaction effect of RAVENIQ and task difficulty.

Fig. 6, Panel C displays the results of a 3way interaction analysis (age, fluid intelligence and task difficulty), we find that the DAN (DLPFC, BA7) and DMN (BA10/MPFC) nodes are all functionally connected during the RAPM. Since this analysis includes both age as well as "Gf" predictors in both RUNS 1 and 3, it is not surprising that we see nodes from BA10/MPFC (predicted by main effect of age) as well as that of the DAN nodes (predicted by main effect "Gf"), as being functionally connected.

To further parse out the results in Fig. 6 (Panel C), we ran a general linear test (functional connectivity analysis- Fig. 6, Panel D) that juxtaposes the key DAN node of BA7 (seeded) against the key DMN node of BA10 (seeded), including the interaction effects of age and "Gf", during the performance of the RAPM in the most challenging RUN3. Significant results ($q < 0.05$), ratify previous results reported in this research, showing an anti-correlation of functional connectivity between the DMN node of BA10/MPFC (deactivation) and the DAN nodes BA7/SPL/precuneus with DLPFC (activation). This result (Panel D, Fig. 6), is effect of the interaction of age and "Gf" on functional connectivity during RUN3 when the brain is challenged with solving the most difficult matrices.

We utilized the 1/3 top and bottom percentiles of participants to selectively examine further the effects of aging on the oldest/youngest participants and that of "Gf" on those participants with highest/lowest RAVENIQ scores. We examined the hemodynamic waveforms of these select participants at the anti-correlated hubs of BA7 (DAN network) and BA10 (DMN network), displayed in Fig. 7.

In Fig. 7 (top bar), at the key RAPM task processing node of BA7 (top bar), we notice that the youngest/highest fluid IQ participants approach the RAPM task head on at a higher effort /percent signal change. The signal attenuates in the middle of a RUN, and finally ramps up the signal peak towards the end of the RUN when the matrices are the most difficult to solve, requiring more effort. In contrast, the oldest adults and those participants with the lowest "Gf", take their time to ramp up effort at the beginning of the RUN. They eventually peak in the middle of the RUN, and finally tend to ramp down effort/ percent signal change towards the end, perhaps giving up on solving the most difficult

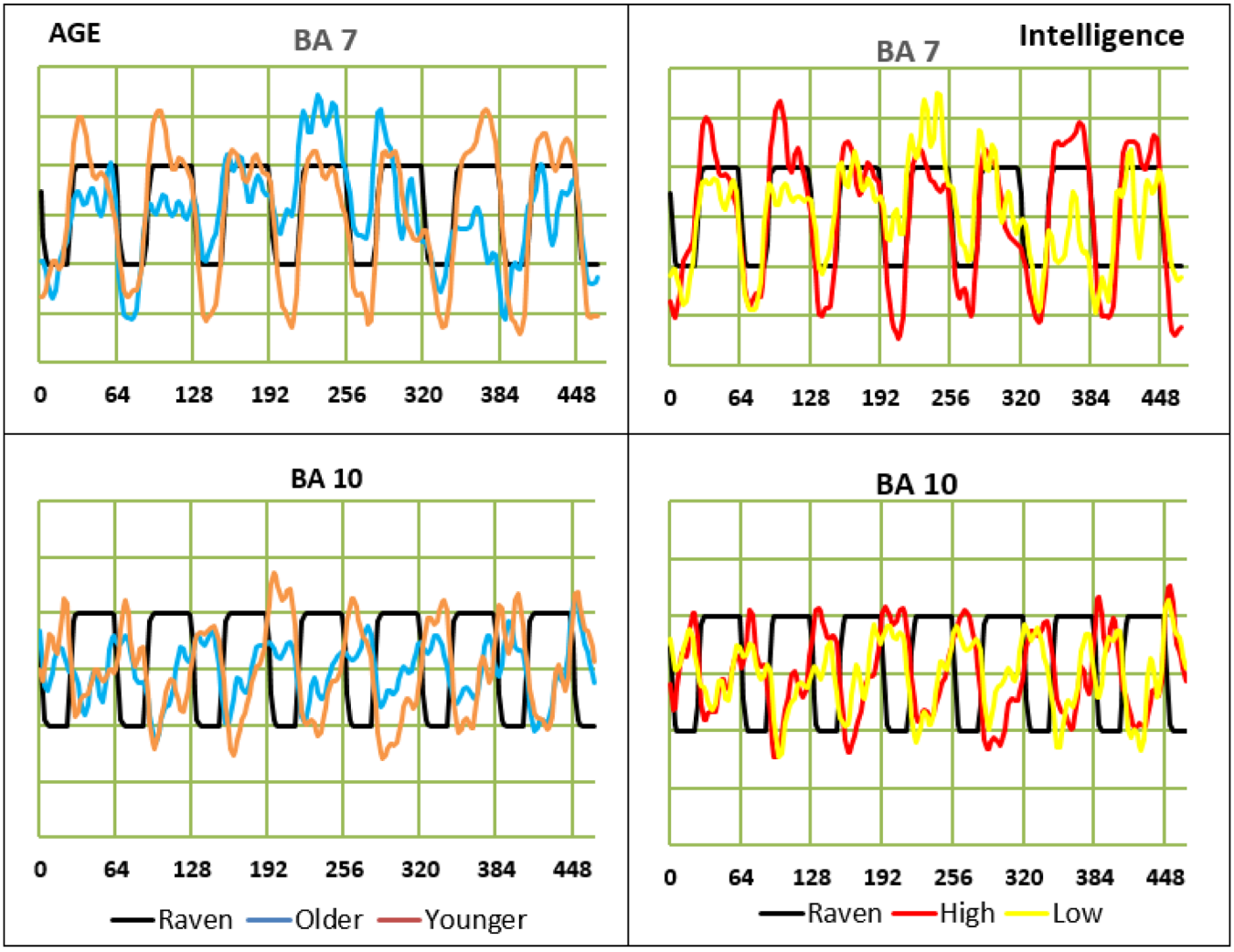

Fig. 7. Effect of age and fluid intelligence on oscillatory waveforms of hemodynamic response at critical nodes (BA7, BA10) for RAPM task performance. The waveforms represent top 1/3rd and bottom 1/3rd of participants' average actual hemodynamic response by age (left bar, Mean = 29.67-years-younger, Mean = 64.71-years-older) and RAVENIQ (right bar, Mean = 10-low, Mean = 15.6-high,) at the anti-correlated hubs of BA 7 (top row) and BA 10 (bottom row) during RAPM/control task performance. All signals are arbitrarily scaled for easy visual comparison around 0 (Y-axis). The X-axis represents time from start of functional scan to completion of RUN 3. The idealized hemodynamic response (IHRF)/block design of the RAPM task (black) forms the backdrop.

matrices at the end of the RUN.

Overall, we see that oldest participants seem less adaptive in modifying signal intensity exhibiting, smaller signal peaks and troughs in the key hubs of BA 7 and BA10 (Fig. 7) to meet task demands as the matrices get harder, when compared to youngest participants. A significant positive correlation between age and BA10 RUN3 (see Table 2) indicates that oldest participants may additionally recruit activity in the prefrontal cortex to assist the DAN nodes in solving the matrix puzzles. This is visually borne out in Fig. 7, where we see in the lower bar representing age, that the oldest participants (blue waveform) activate BA10 to some extent while solving the matrices while the youngest participants exhibit strong signal de-activation/troughs at this time.

To summarize the above results, while the default mode and dorsal attentional networks are well known to be anti-correlated with each other [67], we find in our study that "Gf" predicts BOLD response and increased activation of BA7/superior parietal lobule and DLPFC, key nodes of the DAN network, while solving the matrices, irrespective of task challenge. Age predicts extent of de-activation and functional connectivity between the DMN nodes of BA 10/MPFC and PC irrespective of task challenge. The percent signal change between RUNS 1 and 3 achieve statistical significance only at the BA7 /SPL/precuneus and BA10/MPFC nodes, as evident in the results of the Wilcoxon tests reported in Table 4.

Nevertheless, this does not answer the question of whether there is a global increase in whole-brain percent signal activity between easy and difficult task conditions. If the brain does consume similar extents of metabolic resources when it is performing a relatively easy task (control task) as it does when cognitively taxed (RAPM), then we should see no significant difference in non-normalized whole-brain activity between the control task (very easy) and RAPM RUNS (very difficult). As a secondary analysis, our results indicate in a t-test = −0.003, $p = 0.9977$, no significant difference in the whole brain means of percent signal change during the RAPM (Mean = 801.0773) and control task (Mean = 800.98). This suggests that the brain may maintain equilibrium using neurally efficient mechanisms under varying conditions of cognitive load.

4. Discussion

While early studies [1,2,6,68] suggested that superior cognitive ability depended on the brain's global lower energy consumption and on the efficiency of the brain's intrinsic functional network architecture [69], recent research [36,70] has suggested that this may not be the case. Our findings indicate that neural efficiency may not be dependent,

but rather modified by cognitive intelligence and age, specifically "Gf", which is the fMR measure utilized in this study.

The neural efficiency hypothesis [1] has over time been modified to propose that neural efficiency could be associated with the suppression of unnecessary regions [1,68], thereby enhancing the performance of relevant regions. We identify a similar suppression/ de-activation in the posterior cingulate and MPFC of the DMN network while solving the RAPM, while simultaneously noting a parametric increase of activity in the SPL/BA 7/precuneus and the DLPFC of the DAN network which together may represent a form of distributed neural efficiency. This has been borne out in recent fMR studies of increased activation of the DAN [4,63] and de-activation of the DMN [3,4] networks.

We demonstrate that the activity of specific nodes of the anti-correlated networks of DAN (BA7/superior parietal lobule/precuneus, DLPFC) and DMN (BA10/MPFC, PC), which incur the highest energy costs [30], are modulated by "Gf", age and task difficulty.

According to the NEH [35], those with higher IQ have should be taxed less in both easy and difficult tasks. On the contrary, in our data, we see that those with higher "Gf" (RAVENIQ) are taxed less in the easy RUNS, but expend more effort in the difficult matrices as has later been proposed [6]. This may indicate that in the earlier RUNS, neural capacity [71,72], defined as the maximal activation achieved in the brain that correlates with increasing cognitive load, has not been attained for those individuals higher in fluid intelligence. Fig. 7 (top bar), focused on neural efficiency by age and RAVENIQ, illustrates how at the region of BA7, individuals with the lowest scores on RAVENIQ and those highest in age may achieve neural capacity towards the end of a RUN, when cognitive load is the highest. Towards the end of a RUN in the top bar, their cortical activation falls off and is lower than that of youngest participants and individuals with the highest "Gf". This similarity in cortical activation between the oldest/lowest "Gf" participants could be due to the possibility that the sampling may be from the same subset of participants, since "Gf" is known to decline with age [10,73,74].

Critical to the concept of fluid intelligence is the notion of cognitive flexibility that allows one to engage in novel reasoning or problem solving. This involves the ability to intentionally attend and hold in short-term working memory all the goals of the RAPM task as assigned, as well as the diverse options available, from which one correct response is selected for each matrix. The DLPFC [75] and BA7 [76] are important to working memory, a key component of fluid intelligence in keeping multiple options online while solving the matrices. As the individual comprehends and begins to work through the options, s/he would have to rule out and exclude irrelevant information from her/his attention, and update working memory to focus only on relevant schema. The DLPFC is also a key region, which provides top-down attentional and cognitive control in external task processing [64] and in our dataset is significantly correlated with RAVENIQ in both easy and difficult task conditions. Thus, these two nodes of the DAN network, which are a major substrate of working memory, cognitive control and "Gf" [43], are hence not surprisingly the key areas of increased activation while solving the RAPM.

This task of exploration, updating and narrowing options that are kept active and online towards the goal of solving the matrices, involve both working memory and fluid intelligence [77]. Both and especially the latter are heavily impacted by the aging process [10]. Interestingly, in our data, neither age nor "Gf" has a meaningful relationship with response time in solving the matrix puzzles. Older adults do not seem to be significantly slower, and individuals with higher RAVENIQ do not seem to be significantly faster, in solving the puzzles in our dataset. The lack of a relationship between age and response time is unlike previous theories suggesting that age slows down individuals when they engage in complex cognitive challenges [10]. This may be partially accounted for by the specific instruction they received, to continue thinking about the problem until the 40 s time limit for each puzzle is reached. However, the last finger tap response is well before this time limit for most subjects.

In our research, age (as a secondary effect) compromises extent of activation of the BA7/precuneus node, which is essential to solving the matrices. On the other hand, age significantly predicts the percent signal change and functional connectivity of both DMN hubs of BA10/MPFC and PC. This may indicate a recruitment of these two DMN hubs in problem-solving and to support the DAN hubs, when these individuals are cognitively taxed. In the case of the oldest subgroup, less signal perturbation (Fig. 7) amongst the oldest adults may also be due to greater reliance on experience to solve the RAPM rather than novel or brute computation in the present moment. These two results in opposing directions between age and key nodes of the DAN (negative) and DMN (positive), suggest that the aging brain may struggle to rev up to task demands when challenged. Note that all the peak activated areas in this task are bilateral, perhaps due to compensatory activation of both hemispheres, associated with HAROLD (Hemispheric Asymmetry Reduction in Older adults) model, attributed to older adults [78]. All of these bolster prior evidence [7] that older adults may draw extra resources and rely on the prefrontal cortex (in this case the medial section) to a greater extent, when faced with challenging cognitive tasks.

Research tapping the superior temporal resolution of magnetoencephalography (MEG) has indicated that in visuo-spatial problem-solving, the activation patterns tend to sequence from the posterior visual stream and sensory motor areas to the lateral frontal executive areas where hypotheses testing of the correct solutions/decision-making may be underway [79]. Fig. 4 (Panel D) hints at the involvement/activation of all these areas in the functional connectivity patterns of the DAN network. MEG research is also pointing to individual differences in neural capacity, where those with higher IQ may be activating fewer/different regions than those with lower IQ who may be relying more on frontal executive areas to carry more of the cognitive load, earlier on in the sequence in visuo-spatial problem solving [79]. In our study, this is somewhat mirrored amongst older adults (discussed in the previous paragraph), who may be additionally recruiting the medial frontal areas to assist in solving the puzzles.

The anti-correlation between BA7 and BA10 in RUN3, while solving the RAPM, may represent an oscillatory, high-volume, fast communication and information integration that occurs between flexible hubs [41] of the rich club network with high centrality [37], although these hubs are physically remote in the brain [39,80]. The expanding deactivation at BA10 and PC illustrated in Fig. 3 between RUNS 1 and 3, also suggests that as task difficulty increases, resources from these two DMN nodes may be diverted to the DAN network nodes of DLPFC and superior parietal lobule/precuneus where the matrices are solved.

The inhibition of the DMN when the brain is engaged with external task processing has been attributed to the pMFG in prior research, where simultaneous activation of the aMFG has been attributed to strengthening functional connectivity of DAN nodes [66], which are engaged in external task processing. Thus, in our study we see simultaneous activations of both the anterior and posterior middle frontal gyri while solving the RAPM. This enhanced connectivity between the a/pMFG and BA7 during the RAPM task may bolster and support problem solving. It is possible that the activity in the pMFG during the RAPM triggers transient suppression of the two DMN nodes to provide necessary, extra metabolic resources to the specific DAN nodes of BA7 and DLPFC, in executing this challenging cognitive task.

Additional clues to this transient suppression and recovery of these DMN nodes by pMFG, are seen in Fig. 5, where the wave-forms of BA10/MPFC and PC undergo a sharp dip at the beginning of the RAPM, and when the brain is minimally processing the control task (which is very easy), we see that the DMN nodes of MPFC/BA10 and PC, rise to normal levels instantaneously. During the control task, these DMN nodes are perhaps engaging in intrinsic incubating, coding and updating the freshly learned information [26] from the previous RAPM task item, which may then be applied to the next upcoming challenge. Perhaps this is one example of how the brain achieves and maintains energy equilibrium when it is "on" and "off" extrinsic task processing.

This also suggests that those with the highest "Gf" or those oldest in age may achieve better task performance by borrowing metabolic resources from DMN hubs, which are de-activated, thus allowing the DAN nodes to achieve greater signal intensities and computational power.

If the maintenance of excitation/inhibition (E/I) ratio of glu/GABA at the DMN nodes during baseline REST represents the highest metabolic energy cost for the human brain [21,22,25,49,81], then a mechanism of distributed neural efficiency may allow the brain to enhance glutamate levels (activation) at DAN nodes and enhance GABA/glu ratios (de-activation) at the DMN nodes during external task processing such as RAPM. While this may marginally increase global consumption of metabolic resources, it largely maintains energy homeostasis during this time. Thus, this mechanism of distributed neural efficiency may modulate resource allocation strategies by using a more focused and efficient organization of task-related networks by additionally capitalizing on internal strengths such as fluid intelligence or to compensate for age-related deficits.

The variance in "Gf", age, task difficulty and our ability to control for all of these proposed moderators [6] including education is a strength of this study. A limitation of this research is that it proposes distributed neural efficiency as one viable mechanism of the brain's global homeostasis in resource consumption and metabolic activity, in the context of "Gf" with the use of only one cognitive task and only at the brain circuit/network level of organization. However, early clues of these nodes serving as flexible functional hubs in wide cognitive performance [41,43] are encouraging.

Distributed neural efficiency mechanisms may also allow for efficient redistribution of resources to allow rapid response to task contingencies. This has held true irrespective of the sensorial mode involved, whether visuo-spatial [82] as in our research, or involving multi-modal tasks; and while utilizing testing modes other than fMRI, such as electro encephalography [83–85] or evoked oxygenation of the PFC using near-infrared spectroscopy [86]. Thus, further research has the potential to explore the scope of distributed neural efficiency through (1) multiple testing modes, (2) examining the accuracy of resource consumption in several brain regions and (3) measuring energy consumption efficiency mechanisms at molecular, cellular, neuronal, circuit and network levels of scalar organization during cognitive performance.

Training and education of the elderly has been constrained due to the neurophysiological effects of aging. These aging effects create complex interactions of age, intelligence and aptitude which affect educational methodologies as well as training outcomes [87]. Recent cutting edge research has suggested that functional connectivity patterns of the fronto-parietal network may predict or "finger-print" an individual's "Gf" [88]. Such bio-markers, in the future may serve in the development of unique bio-trackers of training performance in the elderly by also incorporating individual differences such as age, sex, and "Gf" as baseline measures. The development of these behavioral phenotypes have the potential to address learning in the healthy elderly, but also to stave off or track mild or severe cognitive decline in age-related disease.

While the industry for cognitive enhancement through "brain training" continues to proliferate, there is virtually no robust evidence of genuine long-term gains with transfer of learning/performance across domains through these existing methods [79]. Further research and knowledge regarding the layered, hierarchical mechanisms of neural efficiency in the brain may provide leverage in the development of customized cognitive enhancement programs that successfully tap individual differences in learning contingencies.

5. Conclusion

In conclusion, perhaps the brain achieves neural efficiency in a distributed fashion by increasing processing power on demand by diverting resources from other regions within the P-FIT network. It is plausible that neural efficiency is not a simple decrease/increase of global brain resource use in higher-IQ individuals, but also effective allocation of limited resources where and when required to maintain global energy homeostasis. Thus, the brain may spontaneously inhibit those networks that are not critically important in high –IQ individuals to increase computational power; or to recruit additional regions when taxed by age. Task difficulty may also be a moderating variable in determining the extent of de-activation of unnecessary regions. These results may redefine and broaden our understanding of the mechanism of neural efficiency as well as the functional inter-relationships between brain regions that network in the emergence of "g". Our findings proposing that the brain modulates resource allocation strategies based on inherent limitations such as fluid intelligence, age and external task contingencies, may represent one form of neural efficiency employed by the brain at the circuit/network level, amongst many others. These forms of adaptive efficiency that the brain employs have implications for how we may better continuously learn.

Declaration of interests

None

Ethical statement

All participants in the experiments were treated in accordance with APA ethical standards and guidelines for research with human participants.

Financial disclosure

My co-authors and I do not have any financial interests that might be interpreted as influencing the research.

Author contributions

KR conceptualized the research and wrote the paper; KR and EZ analyzed the data; NCA designed the fMR study paradigm and supervised data collection and analysis. All authors discussed the results and contributed significantly to improving the manuscript.

Funding sources

This research has been funded by grants from the Brain and Behavior Research Foundation, Grant IDs No. 13,184 and 19,402; a grant from Defense Advanced Research Projects Agency (DARPA), Grant ID No. FA8650-07-1-7744; and a grant from Nellie Ball Foundation, ID No. 18,518,500.

Acknowledgements

We would like to recognize the efforts of David Ellison, Alane Tranel, Ethan Wykert and Chanel Vidal in data collection and scoring; Charles Kramer's assistance in scripting data analysis, and Daniel Langstraat's assistance in compiling figures and tables.

References

[1] R.J. Haier, B. Siegel, C. Tang, L. Abel, M.S. Buchsbaum, Intelligence and changes in regional cerebral glucose metabolic rate following learning, Intelligence 16 (3) (1992) 415–426.
[2] R.J. Haier, B.V. Siegel Jr, K.H. Nuechterlein, E. Hazlett, J.C. Wu, J. Paek, H.L. Browning, M.S. Buchsbaum, Cortical glucose metabolic rate correlates of abstract reasoning and attention studied with positron emission tomography, Intelligence 12 (2) (1988) 199–217.
[3] I. Lipp, M. Benedek, A. Fink, K. Koschutnig, G. Reishofer, S. Bergner, A. Ischebeck, F. Ebner, A. Neubauer, Investigating neural efficiency in the visuo-spatial domain: an FMRI study, PLoS One 7 (12) (2012) e51316.
[4] U. Basten, C. Stelzel, C.J. Fiebach, Intelligence is differentially related to neural

effort in the task-positive and the task-negative brain network, Intelligence 41 (5) (2013) 517–528.
[5] B. Dunst, M. Benedek, E. Jauk, S. Bergner, K. Koschutnig, M. Sommer, A. Ischebeck, B. Spinath, M. Arendasy, M. Bühner, Neural efficiency as a function of task demands, Intelligence 42 (2014) 22–30.
[6] A.C. Neubauer, A. Fink, Intelligence and neural efficiency, Neurosci. Biobehav. Rev. 33 (7) (2009) 1004–1023.
[7] P.A. Reuter-Lorenz, K.A. Cappell, Neurocognitive aging and the compensation hypothesis, Curr. Dir. Psychol. Sci. 17 (3) (2008) 177–182.
[8] R.B. Cattell, The measurement of adult intelligence, Psychol. Bull. 40 (3) (1943) 153.
[9] J.L. Horn, R.B. Cattell, Age differences in fluid and crystallized intelligence, Acta Psychol. (Amst) 26 (1967) 107–129.
[10] T.A. Salthouse, The processing-speed theory of adult age differences in cognition, Psychol. Rev. 103 (3) (1996) 403.
[11] N. Raz, A.M. Daugherty, Pathways to brain aging and their modifiers: free-radical-induced energetic and neural decline in senescence (FRIENDS) model-A mini-review, Gerontology (2017).
[12] J.C.G. Jr, Factors affecting learning in older adults, Educ. Gerontol. 22 (4) (2006) 359–372.
[13] C.W. Tyler, L.T. Likova, S.C. Nicholas, Analysis of neural-BOLD coupling through four models of the neural metabolic demand, Front. Neurosci. 9 (2015).
[14] J.K. Thompson, M.R. Peterson, R.D. Freeman, Single-neuron activity and tissue oxygenation in the cerebral cortex, Science 299 (5609) (2003) 1070–1072.
[15] J.K. Thompson, M.R. Peterson, R.D. Freeman, High-resolution neurometabolic coupling revealed by focal activation of visual neurons, Nat. Neurosci. 7 (9) (2004) 919–920.
[16] N.K. Logothetis, J. Pauls, M. Augath, T. Trinath, A. Oeltermann, Neurophysiological investigation of the basis of the fMRI signal, Nature 412 (6843) (2001) 150.
[17] L. Sokoloff, R. Mangold, R.L. Wechsler, C. Kennedy, S.S. Kety, The effect of mental arithmetic on cerebral circulation and metabolism, J. Clin. Invest. 34 (7 Pt 1) (1955) 1101.
[18] P.L. Madsen, J.F. Schmidt, S. Holm, H. Jorgensen, G. Wildschiodtz, N.J. Christensen, L. Friberg, S. Vorstrup, N.A. Lassen, Mental stress and cognitive performance do not increase overall level of cerebral O_2 uptake in humans, J. Appl. Physiol. 73 (2) (1992) 420–426.
[19] P. Roland, L. Eriksson, S. Stone-Elander, L. Widen, Does mental activity change the oxidative metabolism of the brain? J. Neurosci. 7 (8) (1987) 2373–2389.
[20] D.D. Clarke, L. Sokoloff, Circulation and energy metabolism of the brain, Basic Neurochem. Mol. Cell. Med. Aspects 6 (1999) 637–669.
[21] L. Yu, Y. Yu, Energy-efficient neural information processing in individual neurons and neuronal networks, J. Neurosci. Res. (2017).
[22] M.E. Raichle, D.A. Gusnard, Appraising the brain's energy budget, Proc. Natl. Acad. Sci. 99 (16) (2002) 10237–10239.
[23] L. Sokoloff, The physiological and biochemical bases of functional brain imaging, Cognit. Neurodyn. 2 (1) (2008) 1–5.
[24] D. Clarke, L. Sokoloff, Circulation and Energy Metabolism in the Brain Basic Neurochemistry, Lippincott-Raven, New York, 1999.
[25] R.G. Shulman, D.L. Rothman, K.L. Behar, F. Hyder, Energetic basis of brain activity: implications for neuroimaging, Trends Neurosci. 27 (8) (2004) 489–495.
[26] M.E. Raichle, Two views of brain function, Trends Cogn. Sci. 14 (4) (2010) 180–190.
[27] M.E. Raichle, The brain's default mode network, Annu. Rev. Neurosci. (0) (2015).
[28] R.L. Buckner, J.R. Andrews-Hanna, D.L. Schacter, The brain's default network, Ann. N. Y. Acad. Sci. 1124 (1) (2008) 1–38.
[29] N.C. Andreasen, D.S. O'Leary, T. Cizadlo, S. Arndt, K. Rezai, G.L. Watkins, L.L. Boles Ponto, R.D. Hichwa, Remembering the past: two facets of episodic memory explored with positron emission tomography, Am. J. Psychiatry 152 (11) (1995) 1576–1585.
[30] S.N. Vaishnavi, A.G. Vlassenko, M.M. RUNdle, A.Z. Snyder, M.A. Mintun, M.E. Raichle, Regional aerobic glycolysis in the human brain, Proc. Natl. Acad. Sci. 107 (41) (2010) 17757–17762.
[31] R.L. Buckner, J.L. Vincent, I. Kahn, A.Z. Snyder, M.E. Raichle, Evidence for a frontoparietal control system, Cereb. Cortex 24 (3) (2014) 773–784.
[32] J. Gläscher, D. Rudrauf, R. Colom, L. Paul, D. Tranel, H. Damasio, R. Adolphs, Distributed neural system for general intelligence revealed by lesion mapping, Proc. Natl. Acad. Sci. 107 (10) (2010) 4705–4709.
[33] Y. Li, Y. Liu, J. Li, W. Qin, K. Li, C. Yu, T. Jiang, Brain anatomical network and intelligence, PLoS Comput. Biol. 5 (5) (2009) e1000395.
[34] J. Gläscher, D. Tranel, L.K. Paul, D. Rudrauf, C. Rorden, A. Hornaday, T. Grabowski, H. Damasio, R. Adolphs, Lesion mapping of cognitive abilities linked to intelligence, Neuron 61 (5) (2009) 681–691.
[35] R.E. Jung, R.J. Haier, The Parieto-Frontal Integration Theory (P-FIT) of intelligence: converging neuroimaging evidence, Behav. Brain Sci. 30 (02) (2007) 135–154.
[36] U. Basten, K. Hilger, C.J. Fiebach, Where smart brains are different: a quantitative meta-analysis of functional and structural brain imaging studies on intelligence, Intelligence 51 (2015) 10–27.
[37] X.-N. Zuo, R. Ehmke, M. Mennes, D. Imperati, F.X. Castellanos, O. Sporns, M.P. Milham, Network centrality in the human functional connectome, Cereb. Cortex 22 (8) (2012) 1862–1875.
[38] Jonathan D. Power, Bradley L. Schlaggar, Christina N. Lessov-Schlaggar, Steven E. Petersen, Evidence for hubs in human functional brain networks, Neuron 79 (4) (2013) 798–813.
[39] G. Collin, O. Sporns, R.C. Mandl, M.P. van den Heuvel, Structural and functional aspects relating to cost and benefit of rich club organization in the human cerebral cortex, Cereb. Cortex (2013) bht064.
[40] M.P. van den Heuvel, R.S. Kahn, J. Goñi, O. Sporns, High-cost, high-capacity backbone for global brain communication, Proc. Natl. Acad. Sci. 109 (28) (2012) 11372–11377.
[41] M.W. Cole, J.R. Reynolds, J.D. Power, G. Repovs, A. Anticevic, T.S. Braver, Multi-task connectivity reveals flexible hubs for adaptive task control, Nat. Neurosci. 16 (9) (2013) 1348–1355.
[42] D. Vatansever, D.K. Menon, A.E. Manktelow, B.J. Sahakian, E.A. Stamatakis, Default mode dynamics for global functional integration, J. Neurosci. 35 (46) (2015) 15254–15262.
[43] M.W. Cole, T. Yarkoni, G. Repovš, A. Anticevic, T.S. Braver, Global connectivity of prefrontal cortex predicts cognitive control and intelligence, J. Neurosci. 32 (26) (2012) 8988–8999.
[44] K. Hilger, M. Ekman, C.J. Fiebach, U. Basten, Efficient hubs in the intelligent brain: nodal efficiency of hub regions in the salience network is associated with general intelligence, Intelligence 60 (2017) 10–25.
[45] A. Roy, R.A. Bernier, J. Wang, M. Benson, J.J. French Jr, D.C. Good, F.G. Hillary, The evolution of cost-efficiency in neural networks during recovery from traumatic brain injury, PLoS One 12 (4) (2017) e0170541.
[46] E. Genç, C. Fraenz, C. Schlüter, P. Friedrich, R. Hossiep, M.C. Voelkle, J.M. Ling, O. Güntürkün, R.E. Jung, Diffusion markers of dendritic density and arborization in gray matter predict differences in intelligence, Nature Commun. 9 (1) (2018) 1905.
[47] A.D. Iordan, K.A. Cooke, K.D. Moored, B. Katz, M. Buschkuehl, S.M. Jaeggi, J. Jonides, S.J. Peltier, T.A. Polk, P.A. Reuter-Lorenz, Aging and network properties: stability over time and links with learning during working memory training, Front. Aging Neurosci. 9 (419) (2018).
[48] R.P. Viviano, N. Raz, P. Yuan, J.S. Damoiseaux, Associations between dynamic functional connectivity and age, metabolic risk, and cognitive performance, Neurobiol. Aging 59 (2017) 135–143.
[49] Y. Takei, K. Fujihara, M. Tagawa, N. Hironaga, J. Near, M. Kasagi, Y. Takahashi, T. Motegi, Y. Suzuki, Y. Aoyama, N. Sakurai, M. Yamaguchi, S. Tobimatsu, K. Ujita, Y. Tsushima, K. Narita, M. Fukuda, The inhibition/excitation ratio related to task-induced oscillatory modulations during a working memory task: a multtimodal-imaging study using MEG and MRS, Neuroimage 128 (2016) 302–315.
[50] A. Marsman, R.C.W. Mandl, D.W.J. Klomp, W. Cahn, R.S. Kahn, P.R. Luijten, H.E. Hulshoff Pol, Intelligence and brain efficiency: investigating the association between working memory performance, glutamate, and GABA, Front. Psychiatry 8 (154) (2017).
[51] R.J. Haier, R.E. Jung, R.A. Yeo, K. Head, M.T. Alkire, The neuroanatomy of general intelligence: sex matters, Neuroimage 25 (1) (2005) 320–327.
[52] R.J. Haier, C.P. Benbow, Sex differences and lateralization in temporal lobe glucose metabolism during mathematical reasoning, Dev. Neuropsychol. 11 (4) (1995) 405–414.
[53] W.D.W.A.I. Scale, (WAIS-III) The psychological corporation, San Antonio, TX (1997).
[54] S. Ogawa, T.-M. Lee, A.R. Kay, D.W. Tank, Brain magnetic resonance imaging with contrast dependent on blood oxygenation, Proc. Natl. Acad. Sci. 87 (24) (1990) 9868–9872.
[55] J.C. Raven, Advanced Progressive Matrices: Sets I and II, HK Lewis, 1962.
[56] W. Schneider, A. Eschman, A. Zuccolotto, E-Prime Reference Guide, Psychology Software Tools, 2002 Incorporated.
[57] R.W. Cox, AFNI: software for analysis and visualization of functional magnetic resonance neuroimages, Comput. Biomed. Res. 29 (3) (1996) 162–173.
[58] T. White, D. O'Leary, V. Magnotta, S. Arndt, M. Flaum, N.C. Andreasen, Anatomic and functional variability: the effects of filter size in group fMRI data analysis, Neuroimage 13 (4) (2001) 577–588.
[59] R.A. Poldrack, Is “efficiency” a useful concept in cognitive neuroscience? Development. Cognit. Neurosci. (2014).
[60] K. Pearson, Mathematical contributions to the theory of evolution. III. Regression, heredity, and panmixia, Philos. Trans. Royal Soc. Ldn. Series A, containing papers of a mathematical or physical character 187 (1896) 253–318.
[61] R. Team, RStudio: Integrated Development for R, RStudio, Inc., Boston, MA, 2015 URL http://www.rstudio.com.
[62] V. Prabhakaran, J.A. Smith, J.E. Desmond, G.H. Glover, J.D. Gabrieli, Neural substrates of fluid reasoning: an fMRI study of neocortical activation during performance of the Raven's Progressive Matrices Test, Cognit. Psychol. 33 (1) (1997) 43–63.
[63] K.H. Lee, Y.Y. Choi, J.R. Gray, S.H. Cho, J.-H. Chae, S. Lee, K. Kim, Neural correlates of superior intelligence: stronger recruitment of posterior parietal cortex, Neuroimage 29 (2) (2006) 578–586.
[64] J. Smallwood, K. Brown, B. Baird, J.W. Schooler, Cooperation between the default mode network and the frontal–parietal network in the production of an internal train of thought, Brain Res. 1428 (2012) 60–70.
[65] I.J. Deary, L. Penke, W. Johnson, The neuroscience of human intelligence differences, Nat. Rev. Neurosci. 11 (3) (2010) 201–211.
[66] A.C. Chen, D.J. Oathes, C. Chang, T. Bradley, Z.-W. Zhou, L.M. Williams, G.H. Glover, K. Deisseroth, A. Etkin, Causal interactions between fronto-parietal central executive and default-mode networks in humans, Proc. Natl. Acad. Sci. 110 (49) (2013) 19944–19949.
[67] M.D. Fox, A.Z. Snyder, J.L. Vincent, M. Corbetta, D.C. Van Essen, M.E. Raichle, The human brain is intrinsically organized into dynamic, anticorrelated functional networks, PNAS 102 (27) (2005) 9673–9678.
[68] R.J. Haier, Biological Basis of Intelligence, The Cambridge handbook of intelligence, 2011, pp. 351–370.
[69] M.P. van den Heuvel, C.J. Stam, R.S. Kahn, H.E.H. Pol, Efficiency of functional brain networks and intellectual performance, J. Neurosci. 29 (23) (2009) 7619–7624.

[70] J.D. Kruschwitz, L. Waller, L.S. Daedelow, H. Walter, I.M. Veer, General, crystallized and fluid intelligence are not associated with functional global network efficiency: a replication study with the human connectome project 1200 data set, Neuroimage 171 (2018) 323–331.
[71] J. Steffener, K. Li, S. Alain, J. Frasnelli, Quantifying neural efficiency and capacity: a differential equation interpretation of polynomial contrasts, arXiv preprint (2016), arXiv:1606.06249.
[72] I.J. Bennett, H.G. Rivera, B. Rypma, Isolating age-group differences in working memory load-related neural activity: assessing the contribution of working memory capacity using a partial-trial fMRI method, Neuroimage 72 (2013) 20–32.
[73] Population 60 Years and Over in the United States 2005-2007 American Community Survey 3-Year Estimates.
[74] D. Rasmussen, C. Eliasmith, A spiking neural model applied to the study of human performance and cognitive decline on Raven's Advanced Progressive Matrices, Intelligence 42 (2014) 53–82.
[75] A.K. Barbey, M. Koenigs, J. Grafman, Dorsolateral prefrontal contributions to human working memory, Cortex 49 (5) (2013) 1195–1205.
[76] M. Koenigs, A.K. Barbey, B.R. Postle, J. Grafman, Superior parietal cortex is critical for the manipulation of information in working memory, J. Neurosci. 29 (47) (2009) 14980–14986.
[77] Z. Shipstead, T.L. Harrison, R.W. Engle, Working memory capacity and fluid intelligence: maintenance and disengagement, Perspect. Psychol. Sci. 11 (6) (2016) 771–799.
[78] M. Berlingeri, L. Danelli, G. Bottini, M. Sberna, E. Paulesu, Reassessing the HAROLD model: is the hemispheric asymmetry reduction in older adults a special case of compensatory-related utilisation of neural circuits? Exp. Brain Res. 224 (3) (2013) 393–410.
[79] by, A. Sitartchouk, A.C. Evans, The Neuroscience of Intelligence, in: Richard J. Haier (Ed.), Elsevier, 2017by.
[80] D.E. Warren, J.D. Power, J. Bruss, N.L. Denburg, E.J. Waldron, H. Sun, S.E. Petersen, D. Tranel, Network measures predict neuropsychological outcome after brain injury, Proceedings of the National Academy of Sciences, 2014 201322173.
[81] D. Tomasi, G.-J. Wang, N.D. Volkow, Energetic cost of brain functional connectivity, Proc. Natl. Acad. Sci. 110 (33) (2013) 13642–13647.
[82] Z. Guo, A. Li, L. Yu, "Neural efficiency" of athletes' brain during visuo-spatial task: an fMRI study on table tennis players, Front. Behav. Neurosci. 11 (2017) 72.
[83] J.-S. Kang, A. Ojha, G. Lee, M. Lee, Difference in brain activation patterns of individuals with high and low intelligence in linguistic and visuo-spatial tasks: an EEG study, Intelligence 61 (Supplement C) (2017) 47–55.
[84] D.W. Shucard, T.J. Covey, J.L. Shucard, Single trial variability of event-related brain potentials as an index of neural efficiency during working memory, in: D.D. Schmorrow, C.M. Fidopiastis (Eds.), Foundations of Augmented Cognition: Neuroergonomics and Operational Neuroscience: 10th International Conference, AC 2016, Held as Part of HCI International 2016, Toronto, ON, Canada, Springer International Publishing, Cham, 2016, pp. 273–283 July 17-22, 2016, Proceedings, Part I.
[85] L. Cocchi, Z. Yang, A. Zalesky, J. Stelzer, L.J. Hearne, L.L. Gollo, J.B. Mattingley, Neural decoding of visual stimuli varies with fluctuations in global network efficiency, Hum. Brain Mapp. 38 (6) (2017) 3069–3080.
[86] S.I. Di Domenico, A.H. Rodrigo, H. Ayaz, M.A. Fournier, A.C. Ruocco, Decision-making conflict and the neural efficiency hypothesis of intelligence: a functional near-infrared spectroscopy investigation, Neuroimage 109 (2015) 307–317.
[87] B.B. Cobb, C.D. Lay, N.M. Bourdet, C.A. Institute, The Relationship Between Chronological Age and Aptitude Test Measures of Advanced-Level Air Traffic Control Trainees, Civil Aerospace Medical Institute, 1971.
[88] E.S. Finn, X. Shen, D. Scheinost, M.D. Rosenberg, J. Huang, M.M. Chun, X. Papademetris, R.T. Constable, Functional connectome fingerprinting: identifying individuals using patterns of brain connectivity, Nat. Neurosci. 18 (2015) 1664.